2-18-2014

Anthropomorphic Breast Phantoms with Physiological Water, Lipid, and Hemoglobin Content for Near-Infrared Spectral Tomography

Kelly E. Michaelsen
Dartmouth College

Venkataramanan Krishnaswamy
Dartmouth College

Adele Shenoy
Dartmouth College

Emily Jordan
Dartmouth College

Brian W. Pogue
Dartmouth College

See next page for additional authors

Journal of Biomedical Optics

SPIEDigitalLibrary.org/jbo

Anthropomorphic breast phantoms with physiological water, lipid, and hemoglobin content for near-infrared spectral tomography

Kelly E. Michaelsen
Venkataramanan Krishnaswamy
Adele Shenoy
Emily Jordan
Brian W. Pogue
Keith D. Paulsen

SPIE

Anthropomorphic breast phantoms with physiological water, lipid, and hemoglobin content for near-infrared spectral tomography

Kelly E. Michaelsen,* Venkataramanan Krishnaswamy, Adele Shenoy, Emily Jordan, Brian W. Pogue, and Keith D. Paulsen
Dartmouth College, Thayer School of Engineering, 14 Engineering Drive, Hanover, New Hampshire, 03755

Abstract. Breast mimicking tissue optical phantoms with sufficient structural integrity to be deployed as stand-alone imaging targets are developed and successfully constructed with biologically relevant concentrations of water, lipid, and blood. The results show excellent material homogeneity and reproducibility with inter- and intra-phantom variability of 3.5 and 3.8%, respectively, for water and lipid concentrations ranging from 15 to 85%. The phantoms were long-lasting and exhibited water and lipid fractions that were consistent to within 5% of their original content when measured 2 weeks after creation. A breast-shaped three-compartment model of adipose, fibroglandular, and malignant tissues was created with water content ranging from 30% for the adipose simulant to 80% for the tumor. Mean measured water content ranged from 30% in simulated adipose to 73% in simulated tumor with the higher water localized to the tumor-like material. This novel heterogeneous phantom design is composed of physiologically relevant concentrations of the major optical absorbers in the breast in the near-infrared wavelengths that should significantly improve imaging system characterization and optimization because the materials have stand-alone structural integrity and can be readily molded into the sizes and shapes of tissues commensurate with clinical breast imaging. [DOI: 10.1117/1.JBO.19.2.026012]

Keywords: biomedical optics; medical imaging; tissues; spectroscopy.

Paper 130701R received Sep. 26, 2013; revised manuscript received Dec. 23, 2013; accepted for publication Jan. 13, 2014; published online Feb. 18, 2014.

1 Introduction

Phantoms play a vital role in the development, validation, and quality control of imaging systems. Clinically, they are recommended for quality management or mandated for technical surveillance to avoid system malfunction and possible adverse effects on patients undergoing examination. In research and development, phantoms are used for early-stage feasibility testing and performance evaluation; they assist in diagnosing errors or underperforming instrumentation, and enable comparisons of data acquired on different imaging systems.

Phantom measurements have certainly been an important part of the development of near-infrared (NIR) spectral tomography (NIRST). NIR light (600 to 1000 nm) is preferentially absorbed by hemoglobin, water, and lipids—tissue chromophores that are often altered in the presence of malignancy.[1–5] Thus, breast imaging using NIRST has been studied extensively, and imaging systems deployed clinically often incorporate a homogeneous calibration phantom. These phantoms provide information on imaging system accuracy by offering an experimental environment where known chromophore concentrations in the phantom can be compared to their recovered (imaged) counterparts, which in turn improves confidence during breast imaging when comparisons to known values are not possible.

Phantoms are typically used in validation studies of system accuracy and repeatability, and can be constructed from resins or plastics. They should be long lasting, homogeneous, durable, and possess optical properties similar to tissue. Extensive work has been reported on the development of these types of phantoms, and several papers review the different materials and scattering agents that are available.[6,7] Measurements from these phantoms should be highly repeatable so that any changes in the data can be attributed to changes in the system. At present, commercial companies exist that produce customized homogeneous phantoms with tissue-like optical properties in a wide range of sizes and material options.[8]

A second type of optical phantom, referred to as an anthropomorphic phantom, is intended to mimic the breast more closely in both physical shape and tissue composition. It is important for investigating an NIRST system's ability to recover tissue chromophores in different concentrations, locations, and sizes within a heterogeneous volume of material with a scale similar to the breast. These phantoms assist in the optimization of data collection and image reconstruction for a given imaging system, as well as in determining which patient populations are most likely to benefit from the technique. Similar to system validation phantoms, durability and repeatability are important. However, maintaining a spectral absorption profile and absorber concentrations similar to those in the tissue of interest is paramount to success in developing an anthropomorphic phantom. To mimic the breast closely, they should be composed of hemoglobin, water, and lipids in varying physiological concentrations and have their central zones more similar to fibroglandular tissue and their outer areas more representative of adipose tissue in concordance with the typical breast parenchymal pattern.[9]

Previous breast-simulating phantoms have been constructed from hemoglobin, water, and intralipid.[10] The latter is typically added not to mimic breast lipid content, but to create optical

*Address all correspondence to: Kelly E. Michaelsen, E-mail: kelly.e.michaelsen.th@dartmouth.edu

0091-3286/2014/$25.00

scattering. Thus, it is used in low concentrations by volume (~1%). These phantoms effectively emulate the tissue optical properties of oxyhemoglobin, and in some cases, deoxyhemoglobin, but they do not represent physiologically relevant water or lipid contents due to their low intralipid percentage.[11–13]

Development of physiologically relevant water and lipid phantoms is especially important for evaluating NIR imaging systems that incorporate wavelengths >900 nm,[14–16] where absorption by these chromophores is more significant than at lower wavelengths where the hemoglobin absorption dominates. Water and lipids are not only the main absorbers at longer optical wavelengths; they also comprise the bulk of breast tissue volume. Accordingly, several groups have described the development of water and lipid phantoms. For example, Merritt et al.[17] correlated a series of water and lipid fractions with magnetic resonance imaging and diffuse optical tomography. Nachabé et al.[18] analyzed water and lipid contents at higher wavelengths. Most recently, Quarto et al.[19] characterized several recipes for phantoms composed of water and lipids with three different emulsification agents.

In this paper, a robust method is reported for creating semi-solid phantoms with physiologically relevant water and lipid volume fractions that have sufficient structural integrity to stand alone. The free-standing character of these phantoms eliminates the confounding effects of light channeling from a housing container[6] and allows anthropomorphic breast shapes and sizes to be created. The breast is typically composed of adipose tissue, ~81% on average,[20] and although adipose tissue is not 100% lipids, it does have a lipid fraction up to 85%;[21] hence, the most accurate breast phantoms should have high lipid content. Here, we investigate the creation of phantoms with lipid contents >70% in a free-form geometry. A major focus is the systematic examination of emulsifiers to provide the physical scaffolding necessary to create anthropomorphic free-standing phantom structures. Combining water and lipid-based phantoms with hemoglobin is also important. Thus, ease of creation, durability, reproducibility, and cost and accessibility of materials are additional factors that served as driving forces for the development of this new optical breast tissue phantom.

2 Materials and Methods

2.1 *Phantom Creation*

2.1.1 *Material testing*

The most effective phantom recipe was found by testing different combinations of lipid, emulsifier, and water. Water was mixed with butter, margarine, olive oil, canola (rapeseed) oil, Crisco® (vegetable oil), and lard. For each of these combinations, a different emulsifier was used: guar gum, soy lecithin, and borax (sodium borate). These emulsification agents were selected because they are ubiquitous, inexpensive, and nontoxic. The components were mixed using a common blender. The liquid mixture was then poured into a small plastic container and refrigerated overnight. Different ratios of fat to water phantoms were created: 30:70; 40:60; 50:50; 60:40, and 70:30, and tested with different concentrations of emulsifiers. These phantoms were then inspected for their malleability and homogeneity. The purpose of these studies was to ensure that semi-solid models could be constructed from a wide range of water and lipid combinations that simulate actual breast tissue.

To determine how the different emulsification agents altered the optical absorption characteristics of the water and lipid combinations, they were mixed separately with liquid (heated) Crisco and water and imaged in a spectrophotometer from 600 to 1000 nm.

2.1.2 *Water and lipid only phantoms*

After experimenting with a number of lipids and emulsifying agents, lard and guar gum were selected and used in all of the following studies. Combinations of 15:85, 25:75, 30:70, 65:35, 60:40, and 50:50 by volume of water:lipids (and vice versa) were measured. Initial work (not shown) involved mixtures closer to 50:50 in content. After satisfactory results were obtained in these cases, phantoms were created that had more extreme water and lipid fractions than are reported here. Additionally, several identical phantoms were constructed using the same procedure to test the repeatability of the procedure, and some phantoms were imaged longitudinally to assess their longevity at time points separated by 2 weeks where the phantom was stored in a dark refrigerator between imaging sessions.

The procedure for creating these phantoms is illustrated in Fig. 1. First, lard was heated until melted (38°C ± 2°C), and then it was added to a mixture of water and 3% guar gum by weight. A handheld, automated mixer was immediately used to stir the ingredients at low and then medium speed settings. This mixture was then poured into containers that were covered in plastic wrap. The phantoms were refrigerated overnight to solidify before being tested with a diffuse optical spectroscopic imaging (DOSI) system.[22] In many cases, these phantoms were imaged the following day with no additional modifications; however, for thicker and larger phantoms, manual mixing using a handheld potato masher was required. Each measurement takes ~2 s, and the phantoms were measured multiple times at different locations to assess heterogeneity. All scans were performed at room temperature.

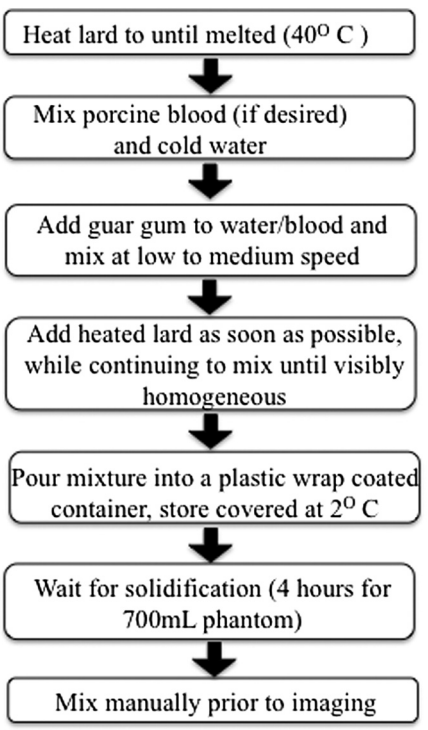

Fig. 1 Schematic of the phantoms creation process.

2.1.3 *Anthropomorphic phantoms*

To create a more anthropomorphic phantom, different components were designed to represent fat, fibroglandular tissue, and tumor, where the first two layers were incorporated into a breast shape mold. Porcine blood was added to phosphate-buffered saline to introduce hemoglobin content. Once the lard was melted, guar gum was added to the blood mixture, and immediately afterward, lard was added while mixing with handheld beaters. The tumor inclusion was formed in a 115-mL container with 80:20 water:lipid ratio and 3% by weight guar gum with 30 μM Hb. To construct the layer representing fibroglandular tissue, a 70:30 water:lipid phantom with 3% by weight guar gum and 20 μM Hb was made having a total volume of 1400 mL. The thickness of this layer was ~4.5 cm. To form the layer that represented fat, a 30:70 water:lipid phantom of total volume 360 mL was made with 3% by weight guar gum and 10 μM Hb. It was 1.3 cm thick. All of the phantoms were refrigerated after mixing. In the case of an anthropomorphic phantom, the remixing step was not necessary because the layers of different compositions were thinner than in the water and lipid only phantoms. Some mixing was performed in the process of adding the tumor inclusion to the fibroglandular layer, as some of the fibroglandular material was removed so that the tumor region could be added.

An anthropomorphic breast-shaped phantom with three distinct tissue regions was imaged in a grid pattern similar to the one used for patient imaging with the DOSI system.[22] The grid pattern consisted of 36 measurement points, each separated by 1 cm in x and y directions and spanning 5×5 cm across the phantom. First, just the fibroglandular-like tissue layer was imaged, then a section 2 cm in depth and diameter was removed from the phantom and replaced with the tumor-like material. The entire phantom was reimaged with measurements acquired from the same positions. Last, a layer of adipose simulating tissue was placed on top of the fibroglandular/tumor layer and the grid pattern of images was repeated.

2.2 *Imaging System*

Measurements were obtained on a DOSI system, currently on loan from the University of California at Irvine as part of a multicenter clinical trial.[23,24] This system possesses both frequency domain and continuous imaging capabilities, which characterize reduced scattering coefficient and absorption across the NIR spectral bandwidth (650 to 1000 nm). The frequency domain components use six distinct wavelengths from 650 to 850 nm, sweeping through modulation frequencies from 50 to 600 MHz with light detected via avalanche photodiodes. The continuous wave portion of the DOSI data samples the tissue at 1024 wavelengths between 580 and 1020 nm spaced ~0.5 nm apart using a broadband white light source and a CCD spectrophotometer. Measurements obtained with this system are reported to be accurate to 0.0006 mm^{-1} for the absorption coefficient and 0.03 mm^{-1} for the reduced scattering coefficient.[25] For the absorption and scattering properties of the phantoms studied here, this accuracy is equal to an error of ~5% in these parameters.

The sample interface is a handheld probe with a fixed-source detector separation of 28 mm. A series of phantom measurements were recorded for calibration prior to sample measurements.[26] For initial experiments, the measurement probe was placed directly on the phantom surface and was cleaned after each measurement. Later, phantoms were wrapped in a very thin layer of plastic to prevent direct contact with the handheld imaging probe. Comparisons of measurements in phantoms with direct contact versus plastic covering showed negligible differences.

2.3 *Data Reconstruction*

A power law fit of the data for the reduced scattering coefficients measured at selected wavelengths defines the scattering properties across the measured range. Chromophore concentrations were calculated using the Beer–Lambert law for the measured absorption coefficients. Molar extinction values for hemoglobin, deoxyhemoglobin, water, and lipids[27–29] were used in this process. Water and lipid fractions were constrained to 100%, and hemoglobin absorption was not considered for the phantoms composed exclusively of water, lard, and emulsifier, but was included for the anthropomorphic phantoms containing porcine blood.

3 Results

3.1 *Creation of Optimal Phantoms*

In creating semisolid phantoms consisting of water and lipids, lipid and emulsifying agents were tested across a range of physiologically relevant water to lipid ratios (30:70 to 70:30) as shown in Fig. 2(a). The amount of emulsifying agent was kept constant for a given volume of phantom to ensure that its effect on optical properties would not vary across different phantom concentrations. As expected, phantoms comprised mostly of water were more gelatinous than phantoms comprised mostly of lipids.

When guar gum was used, all phantoms were semisolid and visually homogeneous. Additionally, guar gum had the lowest signal attenuation in spectrophotometry measurements in the NIR regime of any of the emulsifying agents presented here (data not shown). Thus, it appeared to be the most viable emulsifier for water and lipid phantoms. Several lipid dominant materials underwent spectrophotometry analysis in the NIR range, and Crisco (vegetable oil) and lard (porcine fat) matched published absorption spectra.[28,30] Ultimately, lard was selected for the phantoms as the types and percentages of fatty acid were more similar in the animal fat than the vegetable oil.[31] Despite the addition of an emulsification agent to these phantoms, water and lipid peaks were clearly discernable as shown in Fig. 2(c). The lipid absorption peak is evident in the left graph as a sharp rise around 930 nm, while the water absorption, highlighted in the right graph, has a broad peak above 950 nm that extends to ~1000 nm. The average scattering amplitude of $0.66 \cdot 10^{-3} \lambda\, m^{b-1}$ and average scattering power of 0.42 of the lard-based phantom are on the low end of values found in human subjects.[32]

3.2 *Contrast Sensitivity*

Linear contrast recovery of water and lipids was found when measuring several water:lipid ratios from 15:85 to 85:15, roughly the physiologic limits for the macroscopic tissues probed by diffuse optical techniques.[21] These results are shown in Fig. 3 with an R^2 of 0.998 for the linear fit. Each phantom was measured at 10 distinct locations, and the mean standard deviation of these measurements was 3.5%. However, as noted by other groups,[17,19] lipid content is overestimated,

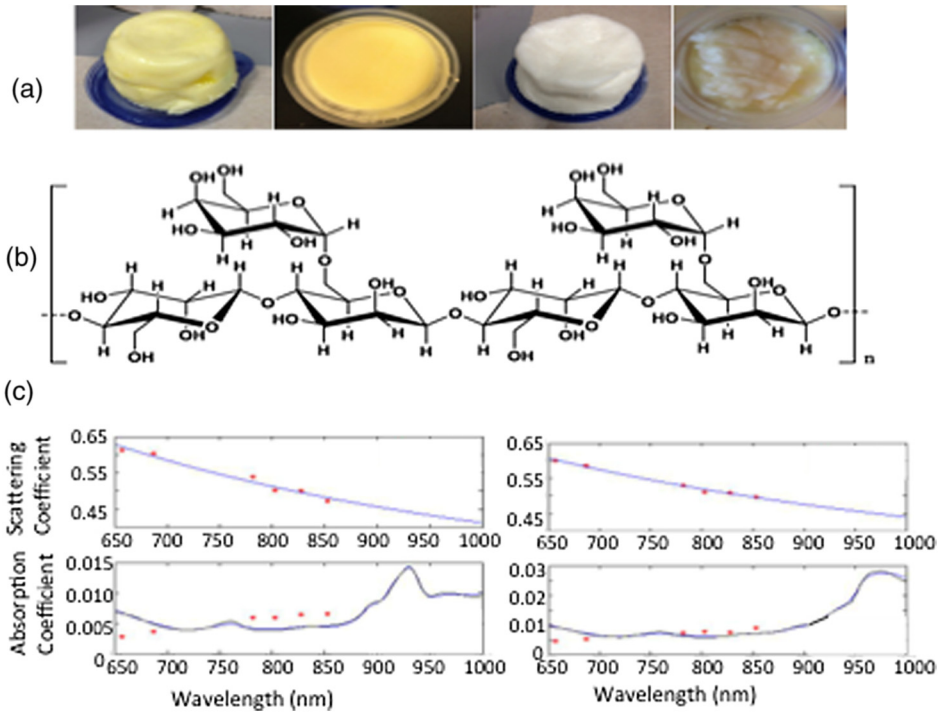

Fig. 2 (a) Several early phantom creations comprised 70% lipid and 30% water. The fats were butter, olive oil, Crisco, and canola oil (left to right). The first and third phantoms included guar gum as the emulsifier, while the second and fourth utilized soy lecithin. (b) The chemical formula for guar gum34. (c) Data from the diffuse optical spectroscopic imaging system for a mostly lipid (left) and mostly water (right) phantom. The top graph shows the scattering data and fits, while the bottom graph shows the absorption results. Specific peaks for lipids and water can be discerned above 900 nm.

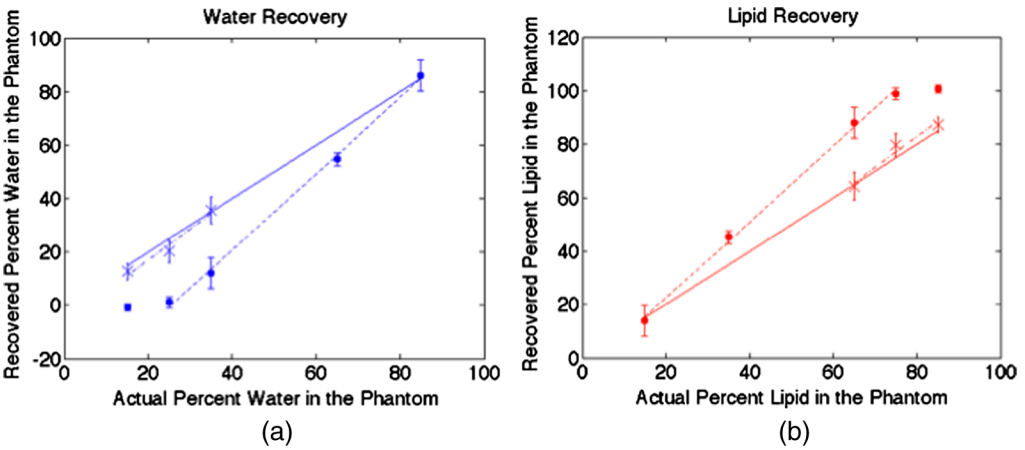

Fig. 3 Graphs of measured water (a) and lipid (b) fractions with (round) data points and standard deviations based on 10 measurements from the top of the phantoms. The dotted line is a linear fit for the phantoms with the higher water content before mixing, exhibiting good linearity. The x-shaped data points and corresponding dashed linear fit for the high lipid content phantoms were obtained after their materials were manually mixed. The solid line depicts the actual water or lipid content.

especially for high lipid ratios. Visual inspection of these phantoms showed a color gradient as observed in the photograph in Fig. 4, and measurements along the side of this phantom demonstrated a decrease in lipid content from the top to the bottom. These phantoms were subsequently remixed manually and then remeasured. The recovered water and lipid content were again linear with an R^2 of 0.96, but with recovered values within 2.5% of their actual values on average as shown by the dashed line in Fig. 3. They maintained homogeneity as well with an average standard deviation of 4.1%. The phantom constituents do not separate after manual remixing as long as the phantoms, once fully formed, are maintained at room temperature or colder, so only a single remixing step is required.

3.3 *Reproducibility*

In order to test the reproducibility of the phantom creation process, three phantoms composed of the same volume of water,

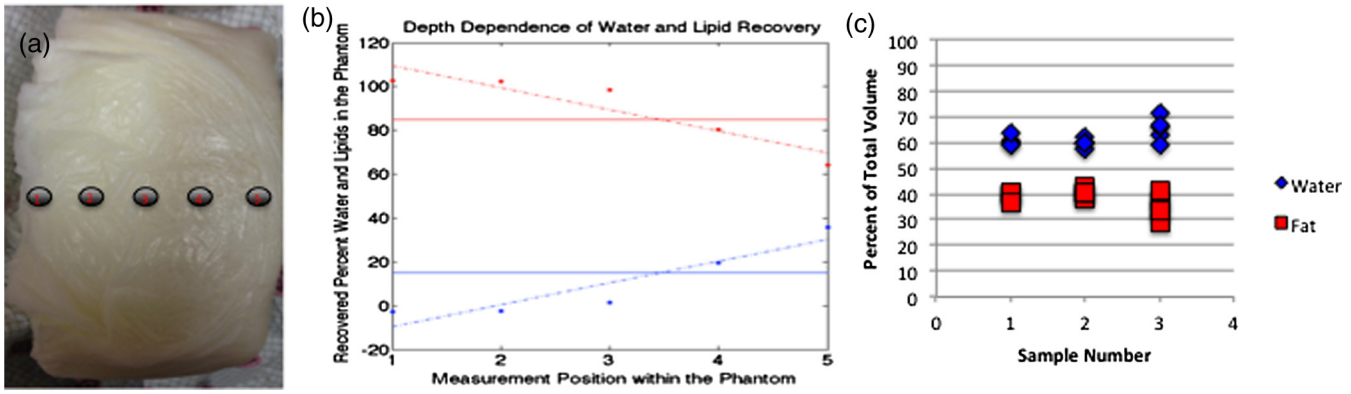

Fig. 4 (a) Photograph showing visible differences between the top (left) and bottom (right) of the phantom. (b) Corresponding depth-dependent measurements confirming the greater presence of lipids at the top of the phantom and higher water at the bottom of the phantom. (c) Repeatability of the phantom creation process in three independently constructed phantoms with the same water and lipid ratio, each measured five times.

lard, and guar gum were fabricated. Each phantom was created by independently following the steps shown in Fig. 1, but all three used ingredients from the same containers and were made by the same individual. The results of this study are shown in Fig. 4(c). The recovered lipid contents were 60.7, 59.7, and 65.0% for the three samples and had intraphantom standard deviations of 1.97, 1.60, and 4.72%, respectively, and interphantom standard deviation of 3.81%.

3.4 *Durability*

Phantoms were evaluated at a variety of time points after initial creation. Because of the need for cooling, no phantoms were tested without at least 4 h of refrigeration. Three phantoms with 15:85, 25:75, and 35:65 water:lipid contents were tested after 2 weeks of refrigeration. At the time of creation, the recovered lipid content was 87.9, 72.1, and 65.8%, respectively. Two weeks later, the values were 87.3, 79.7, and 64.3%, respectively. After an additional week of refrigeration, some phantoms developed mold, indicating that with proper refrigeration these phantoms may last for several weeks.

3.5 *Anthropomorphic Test Case*

The average water content of the fibroglandular simulating layer was measured as 54.9%, 72.8% for the tumor layer prior to insertion in the multilayer phantom, and 29.5% for the adipose layer. As shown in Fig. 5, the tumor inclusion was recovered with 16% greater water content when compared to the fibroglandular region. The actual tumor water content was 10% greater than its fibroglandular counterpart. The adipose region was recovered with a water content within 0.5% of the actual amount. After the tumor region was included in the phantom, measurements in that area showed higher water content and lower lipid content than the surrounding measurement points. Additionally, after the adipose layer was placed on top of the other two, measured water content decreased and lipid content increased as expected. Hemoglobin recovery was 33.2, 25.5, and 8.2 μm for the tumor, fibroglanduar, and adipose regions, respectively, relative to the actual amount of hemoglobin added, i.e., 30, 20, and 10 μm Hb in each of the three tissue types.

4 Discussion

After testing several types of emulsification agents and lipids, guar gum and lard were selected as the ideal constituents for creating breast mimicking phantoms. Lard was preferable, as animal fat is likely more similar to the adipose content in human tissue relative to vegetable-oil-based products. However, the percent of different types of fatty acids contained in the lard can change depending on the animal's diet and the part of the animal from which the fat was contributed.[33] Regardless, changes in the near-infrared absorption due to different fatty acid composition are very small,[31] indicating that both Crisco and lard could be used depending on their availability. To minimize the effects of impurities, all samples produced on a given day were constructed from the same batch of melted lard.

Guar gum showed the lowest absorption in spectrophotometry studies and had the greatest thickening power and homogeneity in phantom formation—characteristics that can be understood from its molecular structure. Guar gum is a high molecular weight polysaccharide composed of highly branched galactose and mannose units.[34] The chemical formula for guar gum is shown in Fig. 2(b). Additionally, examinations of the absorption spectra of phantoms composed of water, lipids, and emulsifier exhibited easily discernable peaks for their water and lipid constituents as shown in Fig. 2(c), and accurate chromophore recovery occurred as demonstrated in Fig. 3.

Water and lipids do not mix spontaneously, but vigorous mixing can create an emulsion, although the two will separate again shortly thereafter. The large size and abundance of branches and hydroxyl groups on the guar gum creates bonds that decrease molecular movement after mixing, thus creating a stable emulsion that is thickened and more solid than the liquid components. Last, cooling after mixing further inhibits separation of water and lipids, and enhances the solidity of the phantom. The final product is moldable, and retains its shape after application of minimal pressure.

This process is not infallible, as some separation of lipid and water may occur as the phantom begins to solidify, causing the linear concentration gradients shown in Fig. 4. The effect is a result of the time delay between the mixing and solidification of the phantom. Procedures exist to mitigate these effects. One method is postrefrigeration manual mixing, which was

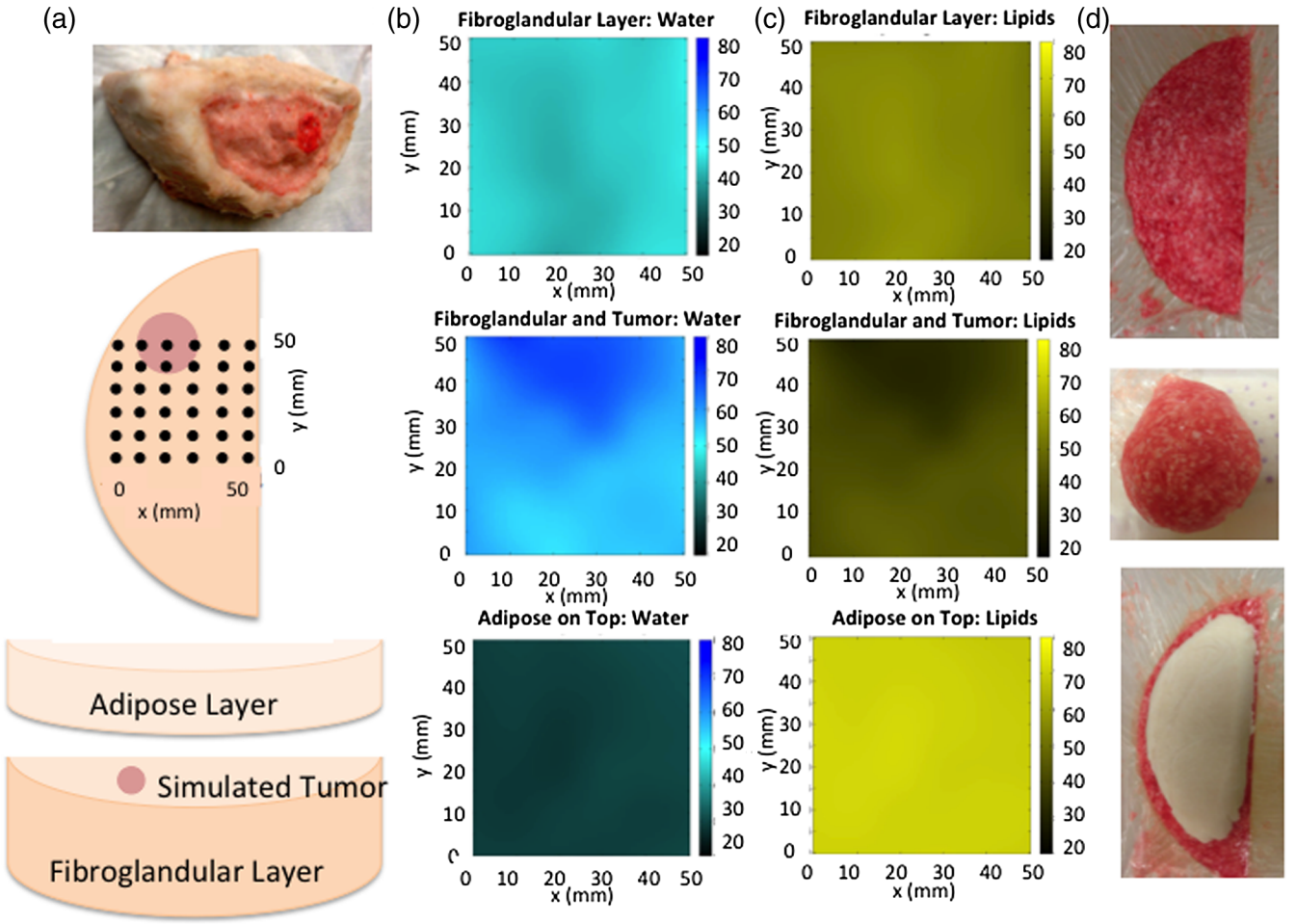

Fig. 5 (a) Schematic of a free-standing three-compartment phantom and the grid pattern used to assess its optical properties. A given phantom was evaluated at 36 locations on a 1-cm grid pattern as shown. Interpolated results across the 5×5 cm grid of individual measurements of optical properties are shown for water in (b) and lipids in (c) in the fibroglandular, tumor, and adipose regions. In the top row, the fibroglandular-simulating phantom was measured alone. The middle row depicts results when a tumor-like inclusion of ~2 cm diameter was added near 20 to 40 mm in x and 60 mm in y directions. In the bottom row, measurement data are shown when a uniform adipose simulating layer was added on top of the fibroglandular and tumor phantom. Photographs of the phantom regions are shown in (d).

very successful as shown in the data and dashed line in Fig. 3, and significantly improved the accuracy of the water and lipid quantification of the mixed material when compared to the same measurements on the unmixed material. Mixing techniques can have an impact on the final phantom outcome. Manual mixing involves slow, gentle compression of the materials at room temperature by hand for a few minutes (the amount of time can vary depending on the size of the phantom), not at high speed, as blending the solid phantom may introduce air bubbles that would alter the desired optical properties. When different individuals mixed the same phantom, average differences in measured water and lipid content were <5%.

Other steps that could be taken include minimizing the height of the phantom, mixing the heated lipids with cold water to decrease the time for solidification, or cooling the mixture more quickly. The first strategy was successful when making the thin adipose layer, whereas the other approaches were not investigated in this study, but would likely improve results in future phantom experiments.

These phantoms possess intrinsic scattering properties resulting from their water and lipid interfaces, which change with concentration. Specifically, higher fat content leads to greater scattering. This behavior is opposite to the scattering found in breast tissue, possibly because tissue water is mostly found within cells that also possess a number of light scattering organelles, whereas these phantoms are composed of pure water with no additional scatterers. Differences in scattering, in addition to differences in absorption, are accounted for in the frequency domain instrumentation.

Despite this water-lipid separation issue, creating durable, homogeneous, repeatable semisolid phantoms across a broad range of water-to-lipid ratios with easily accessible ingredients and tools was demonstrated. Inter- and intraphantom variability was <5%. The phantoms do not break and can be remolded into different shapes as needed, unlike agar or gelatin materials that often crack. They can be compressed with manual force (more easily for higher water content but possible at all compositions), unlike hard resin phantoms. Phantoms measured 2 weeks after creation exhibited water and lipid contents within 5% of their originally measured concentrations. Their semisolid consistency eliminates the complexities of imaging phantoms within containers where light channeling may occur. These phantoms

were inexpensive to construct, costing <5.00 per 700 mL of phantom material, and all of the ingredients and equipment could be purchased at a local grocery store.

An anthropomorphic breast-shaped phantom with three distinct tissue regions was studied as a test case. It contained the three main light absorbers in the NIR—hemoglobin, water, and lipid—and possessed intrinsic scattering properties, albeit on the lower end of what is expected for human breast because its materials do not contain human cells or organelles. Because the melting point of lard is well below the temperature of hemoglobin denaturation, blood can easily be incorporated into this phantom.[35] Adding hemoglobin to the water and lipid phantoms did not substantially alter their water and lipid fractions. Fat content was overestimated in the fibroglandular and tumor phantom sections by ∼15 and 8%, respectively, likely due to the thickness of these compartments (postrefrigeration mixing was not performed in this case) but was <1% in error in the adipose layer. The tumor can be localized when added to the fibroglandular background as shown in Fig. 5. This example demonstrates the feasibility of producing physiologically relevant NIR phantoms composed mainly of water, lipid, and blood that have sufficient structural integrity to be used without any other supporting containers or fixtures.

5 Conclusions

The phantom process described here can be used to create accurate breast-like optical phantoms with matching biological composition and physical shape that have sufficient structural integrity to be used as stand-alone imaging targets. Linear recovery of water and lipid concentrations has been found for compositions between 15 and 85% with errors of <5% of the actual amounts when postrefrigeration mixing was performed. Blood can readily be added to these phantoms, which are then composed of physiologically relevant percentages of the three major absorbers in the NIR regime. The phantoms are moldable and easily shaped by the user. They are also durable, long-lasting and repeatable, easy to make, and inexpensive.

Given the positive characteristics of these phantoms, several areas of research could benefit from their construction. For example, these phantoms can be used for evaluating imaging systems that obtain limited spectral information above 900 nm in order to understand their sensitivity to water and lipid contrast. Alternatively, a multicompartment phantom model of different tissue types can be used to test region-based reconstructions for tomographic imaging systems as well as to assess signal-to-noise characteristics in an optically heterogeneous environment. The semisolid character of these phantoms is useful for testing the effects of different breast shapes and sizes on patient interfaces and at tissue boundaries. Use of these phantoms, which closely mimic tissue optical properties, can provide information to help optimize imaging system development and determine which patients can be successfully imaged on those systems.

Acknowledgments

The authors would like to acknowledge collaborators at the University of California at Irvine for permitting the use of a diffuse optical spectroscopic imaging system for this work as well as John Winn, professor of chemistry at Dartmouth College, for his physical chemistry advice. This work was funded by National Institutes of Health grants R01CA139449 and F30CA168079.

References

1. Q. Fang et al., "Combined optical and x-ray tomosynthesis breast imaging," *Radiology* **258**(1), 89–97 (2011).
2. B. J. Tromberg et al., "Non-invasive in vivo characterization of breast tumors using photon migration spectroscopy," *Neoplasia* **2**(1–2), 26–40 (2000).
3. S. P. Poplack et al., "Electromagnetic breast imaging: results of a pilot study in women with abnormal mammograms," *Radiology* **243**(2), 350–359 (2007).
4. M. G. Pakalniskis et al., "Tumor angiogenesis change estimated by using diffuse optical spectroscopic tomography: demonstrated correlation in women undergoing neoadjuvant chemotherapy for invasive breast cancer?," *Radiology* **259**(2), 365–374 (2011).
5. X. Intes, "Time-domain optical mammography SoftScan: initial results," *Acad. Radiol.* **12**(8), 934–947 (2005).
6. B. W. Pogue and M. S. Patterson, "Review of tissue simulating phantoms for optical spectroscopy, imaging and dosimetry," *J. Biomed. Opt.* **11**(4), 041102 (2006).
7. J. Hwang, J. C. Ramella-Roman, and R. Nordstrom, "Introduction: feature issue on phantoms for the performance evaluation and validation of optical medical imaging devices," *Biomed. Opt. Express* **3**(6), 1399–1403 (2012).
8. J. P. Bouchard et al., "Reference optical phantoms for diffuse optical spectroscopy. Part 1—Error analysis of a time resolved transmittance characterization method," *Opt. Express* **18**(11), 11495–11507 (2010).
9. S. Thomsen and D. Tatman, "Physiological and pathological factors of human breast disease that can influence optical diagnosis," *Ann. N. Y. Acad. Sci.* **838**, 171–193 (1998).
10. R. Michels, F. Foschum, and A. Kienle, "Optical properties of fat emulsions," *Opt. Express* **16**(8), 5907–5925 (2008).
11. T. O. McBride et al., "Spectroscopic diffuse optical tomography for the quantitative assessment of hemoglobin concentration and oxygen saturation in breast tissue," *Appl. Opt.* **38**(25), 5480–5490 (1999).
12. M. A. Mastanduno et al., "Automatic and robust calibration of optical detector arrays for biomedical diffuse optical spectroscopy," *Biomed. Opt. Express* **3**(10), 2339–2352 (2012).
13. K. Michaelsen et al., "Near-infrared spectral tomography integrated with digital breast tomosynthesis: effects of tissue scattering on optical data acquisition design," *Med. Phys.* **39**(7), 4579–4587 (2012).
14. L. Spinelli et al., "Characterization of female breast lesions from multi-wavelength time-resolved optical mammography," *Phys. Med. Biol.* **50**(11), 2489–2502 (2005).
15. J. Wang et al., "In vivo quantitative imaging of normal and cancerous breast tissue using broadband diffuse optical tomography," *Med. Phys.* **37**(7), 3715–3724 (2010).
16. V. Krishnaswamy et al., "A digital x-ray tomosynthesis coupled near infrared spectral tomography system for dual-modality breast imaging," *Opt. Express* **20**(17), 19125–19136 (2012).
17. S. Merritt et al., "Comparison of water and lipid content measurements using diffuse optical spectroscopy and MRI in emulsion phantoms," *Technol. Cancer Res. Treat.* **2**(6), 563–569 (2003).
18. R. Nachabé et al., "Estimation of biological chromophores using diffuse optical spectroscopy: benefit of extending the UV-VIS wavelength range to include 1000 to 1600 nm," *Biomed. Opt. Express* **1**(5), 1432–1442 (2010).
19. G. Quarto et al., "Comparison of organic phantom recipes and characterization by time-resolved diffuse optical spectroscopy," *Proc. SPIE* **8799**, 879905 (2013).
20. T. R. Nelson et al., "Classification of breast computed tomography data," *Med. Phys.* **35**(3), 1078–1086 (2008).
21. S. J. Graham et al., "Changes in fibroglandular volume and water content of breast tissue during the menstrual cycle observed by MR imaging at 1.5 t," *J. Magn. Reson. Imaging* **5**(6), 695–701 (1995).
22. W. Tanamai et al., "Diffuse optical spectroscopy measurements of healing in breast tissue after core biopsy: case study," *J. Biomed. Opt.* **14**(1), 014024 (2009).
23. A. E. Cerussi et al., "Diffuse optical spectroscopic imaging correlates with final pathological response in breast cancer neoadjuvant chemotherapy," *Philos. Trans. Math. Phys. Eng. Sci.* **369**(1955), 4512–4530 (2011).
24. A. Cerussi et al., "In vivo absorption, scattering, and physiologic properties of 58 malignant breast tumors determined by broadband diffuse optical spectroscopy," *J Biomed. Opt.* **11**(4), 044005 (2006).

25. K. S. No et al., "Design and testing of a miniature broadband frequency domain photon migration instrument," *J. Biomed. Opt.* **13**(5), 050509 (2008).
26. A. E. Cerussi et al., "Tissue phantoms in multicenter clinical trials for diffuse optical technologies," *Biomed. Opt. Express* **3**(5), 966–971 (2012).
27. L. Kou, D. Labrie, and P. Chylek, "Refractive indices of water and ice in the 0.65- to 2.5-μm spectral range," *Appl. Opt.* **32**, 3531–3540 (1993).
28. C. Eker, "Optical characterization of tissue for medical diagnostics," Doctoral Thesis, Department of Physics, Lund Institute of Technology (1999).
29. W. G. Zijlstra, A. Buursma, and O. W. van Assendelft, *Visible and Near Infrared Absorption Spectra of Human and Animal Haemoglobin: Determination and Application* VSP (2000).
30. R. L. P. Van Veen et al., "Determination of visible near-IR absorption coefficients of mammalian fat using time- and spatially resolved diffuse reflectance and transmission spectroscopy," *J. Biomed. Opt.* **10**(5), 054004 (2005).
31. C.-L. Tsai, J.-C. Chen, and W.-J. Wang, "Near-infrared absorption property of biological soft tissue constituents," *J. Med. Biol. Eng.* **21**(1), 7–14 (2001).
32. B. Brooksby et al., "Imaging breast adipose and fibroglandular tissue molecular signatures by using hybrid MRI-guided near-infrared spectral tomography," *Proc. Natl. Acad. Sci. U S A* **103**, 8828–8833 (2006).
33. D. E. Koch et al., "Effect of diet on the fatty acid composition of pork fat," *J. Anim. Sci.* **27**(2), 360–365 (1968).
34. Y. Kawamura, Guar Gum: Chemical and Technical Assessment, http://www.fao.org/fileadmin/templates/agns/pdf/jecfa/cta/69/Guar_gum.pdf (2008).
35. R. F. Rieder, "Hemoglobin stability: observations on the denaturation of normal and abnormal hemoglobins by oxidant dyes, heat, and alkali," *J. Clin. Invest.* **49**, 2369–2376 (1970).

Kelly E. Michaelsen is an MD/PhD candidate currently working toward a PhD in biomedical engineering at the Thayer School of Engineering. She graduated from Dartmouth College with honors, majoring in physics and minoring in chemistry while pursuing research in particle physics. She is interested in developing imaging methods that translate into more effective screening, diagnosis, and treatment of disease. Her current research focuses on combining x-ray and optical imaging modalities for breast cancer surveillance.

Venkataramanan Krishnaswamy received his PhD in optical science and engineering from the University of Alabama in Huntsville with specialization in optical systems design and engineering. He is currently a research faculty member at the Thayer School of Engineering, Dartmouth College. His current areas of research include imaging localized tissue scatter response using structured light and dark-field confocal spectroscopy approaches and multimodal imaging systems development combining near-infrared spectral tomography with mainstream clinical imaging modalities.

Adele Shenoy is an undergraduate student at Dartmouth College pursuing a degree in economics while fulfilling the premedical requirements. As a Women in Science Scholar, Presidential Scholar, and Undergraduate Research Scholar, she has been deeply involved in the development, testing, and optimization of optical phantoms for a combined near-infrared and breast tomosynthesis imaging system.

Emily Jordan is an undergraduate student at Dartmouth College majoring in music and minoring in Italian studies and completing the premedical curriculum. As a research associate, her work focuses on optical phantom development, hardware design, human subject interfaces, and imaging.

Brian W. Pogue is a professor of engineering, physics, and astronomy at Dartmouth College, and adjunct professor of surgery at the Geisel School of Medicine. His research is in optical imaging systems, with a focus on molecular and structural imaging of cancer for surgical guidance and imaging radiation therapy. He has published 240 peer-reviewed papers. His research is funded by the National Cancer Institute, and he is a fellow of the Optical Society of America.

Keith D. Paulsen is currently the Robert A. Pritzker professor of biomedical engineering at the Thayer School of Engineering at Dartmouth, professor of radiology at the Geisel School of Medicine, and director of the Advanced Imaging Center at Dartmouth Hitchcock Medical Center. His research has focused on the development and translation of advanced imaging technology, primarily for cancer detection, diagnosis, therapy monitoring, and surgical guidance. He has authored more than 350 archival publications with an active research program, continuously funded by the National Institutes of Health for 25 years.